

Cite this: *Soft Matter*, 2012, **8**, 10914

www.rsc.org/softmatter

PAPER

Mesomorphic and ion conducting properties of dialkyl(1,4-phenylene) diimidazolium salts†

Nadim Noujeim, Salim Samsam, Ludovic Eberlin, Samantha H. Sanon, Dominic Rochefort and Andreea R. Schmitzer*

Received 25th May 2012, Accepted 15th August 2012

DOI: 10.1039/c2sm26213d

A new family of dialkyl(1,4-phenylene)diimidazolium salts has been synthesized. Salts containing triflate and *bis*(trifluoromethanesulfonyl)imide anions and different alkyl chains have been prepared. The molecular structures of didodecyl(1,4-phenylene)diimidazolium triflate and *bis*(trifluoromethylsulfonyl)imide salts were determined by single crystal X-ray diffraction, and the mesomorphic and ionic conducting properties of all these compounds were investigated and are reported here.

Introduction

One of the major goals of materials science is the development of anisotropic ion-conductive materials. Ionic liquids (ILs) have shown many useful properties such as high thermal and chemical stability, low volatility, non-flammability and a wide electrochemical window.¹ Imidazolium-based ionic liquids are well known and have already found wide applications in electrochemical devices, ion transport systems and dye-sensitized solar cells.² Some imidazolium-based ILs have also recently been shown to be useful in catalysis, either as solvents for bioorganic catalysis³ or as emulsion regulators in biphasic processes.⁴ In an attempt to translate the benefits of ILs to the ion-conductive materials, polymer electrolytes, ionogels and ionic liquid crystals have been recently developed.

Different polymer electrolytes obtained by polymerization of ILs,⁵ inclusion of different polymers in ionic liquids,⁶ ionic liquid–polyelectrolyte systems,⁷ and polymer gel electrolytes containing hydrophilic and hydrophobic ionic liquids,⁸ have been reported to possess high conductivity suitable for different applications.

Ion gels, which have the main properties of ILs except outflow, represent a promising family of solid electrolyte membranes, which gives access to a large panel of devices and potential applications as lithium batteries, fuel cells and dye sensitized solar cells.⁹ However, polymer electrolytes and ionogels do not present any conductive anisotropy. There is still a challenging need for obtaining stable materials over time and allowing their use at temperatures much higher than ambient, while presenting anisotropic conductive properties.

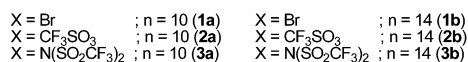
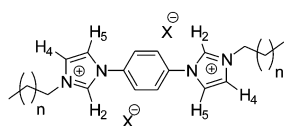
Recently, imidazolium-based thermotropic and lyotropic ionic liquid crystals (ILCs) were reported.¹⁰ These imidazolium-based ILCs were obtained by combining the self-organization properties of liquid crystals (LCs) with the unique solvent properties and ion-conducting properties of imidazolium ILs. The properties of ILCs can be significantly different from those of conventional liquid crystals,¹¹ and more specifically, the properties of imidazolium-based ILCs can also drastically change depending on the molecular architecture and the counterion used. More importantly, development of ILCs led to the achievement of anisotropic ionic conductivity through macroscopically aligning the ionic channels.

Imidazolium-based ILCs can currently be classified into three main categories that overlap to some extent: firstly, ILCs comprised of an imidazolium moiety with one or two alkyl chains¹² incorporating in some cases an aromatic ring generally exhibit smectic mesophases. The imidazolium moiety can also directly be part of the rigid core unit and smectic phases are generally obtained when an alkyl chain is attached.¹³ The second category is comprised of taper shaped imidazolium salts with multiple alkyl chains,¹⁴ with properties related to their strong amphiphilic character and space filling of the lipophilic chains. The third category is comprised of rod like and disc like mesogens containing one or several imidazolium units that are connected to each other by long flexible spacers,¹⁵ where smectic and columnar phases are usually obtained.

We report here the synthesis and study of a symmetrical type of imidazolium-based ILC in which the rigid core is composed of a diimidazolium 1,4-disubstituted phenyl ring with two long alkyl chains attached to this central core, one on each imidazolium moiety. The length of the alkyl chains and the nature of the counterion were varied in order to investigate their influence on the mesomorphic properties and ion conducting properties of these salts (Scheme 1).

Département de Chimie, Université de Montréal, 2900 Edouard Montpetit CP 6128 Succursale centre ville, Montréal H3C3J7, Qc, Canada. E-mail: ar.schmitzer@umontreal.ca; Fax: +1 514-343-7586; Tel: +1 514-343-6744

† Electronic supplementary information (ESI) available: CCDC 884299 and 884300. For ESI and crystallographic data in CIF or other electronic format see DOI: 10.1039/c2sm26213d



Scheme 1 Dialkyl(1,4-phenylene)diimidazolium salts.

Results and discussion

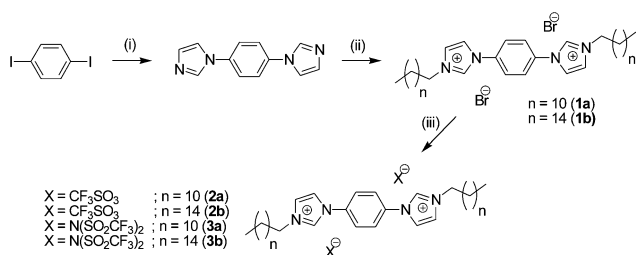
Synthesis

We previously reported the synthesis and supramolecular assemblies of dialkyl(1,4-phenylene)diimidazolium bromide salts with short alkyl chains.¹⁶ These compounds did not exhibit any mesomorphic properties. Furthermore, by increasing the length of the alkyl chains while keeping bromide counterions, it was still not possible to obtain mesomorphic materials. It was only when simultaneously changing both the counterions and increasing the alkyl sidechains (to at least twelve carbons) that compounds displaying LC properties were obtained. The mesophases were stable in a very large temperature range depending on the counterion used.

These compounds were synthesized in a three-step procedure. The first step is a copper(i) catalyzed Ullman-type coupling carried out in anhydrous acetonitrile. The second step is a double nucleophilic substitution of either 1-bromododecane or 1-bromohexadecane on the diimidazole intermediate. This step yielded dialkyl(1,4-phenylene)diimidazolium bromide salts **1a** and **1b** which were engaged in anion metathesis to afford compounds **2a** and **2b**, and **3a** and **3b** (Scheme 2). All the salts were air stable and were characterized by ¹H, ¹³C NMR and high resolution mass spectrometry.

Solid state organization of 2a and 3a

The single crystal X-ray structures of compounds **2a** and **3a** were obtained and investigated to understand the supramolecular organization of these salts in the solid state. For compound **2a**, the predominant supramolecular interactions observed in the crystal are the hydrophobic interactions between the alkyl chains and the H-bonds between the acidic H2 imidazolium proton and the oxygen atom of the triflate (TfO) anion. No π -stacking or T-stacking was observed in this crystal structure, which is usually



Scheme 2 Synthesis of the dialkyl(1,4-phenylene)diimidazolium salts. (i) Cs₂CO₃, imidazole, Cu₂O, salicylaldehyde, acetonitrile, reflux, 48 h, 81%; (ii) alkyl bromide, acetonitrile, reflux, 12 h, 95–99%; (iii) NH₄CF₃SO₃ or LiN(SO₂CF₃)₂, water–methanol, r.t. 30 min 67–88%.

very common for this type of diimidazolium salts, as previously described by our research group.¹⁷ For compound **2a**, the alkyl chains are separated from each other by 4.4 Å in the (*bc*) plane, and by 8.5 Å along the (*a*) axis, which shows a lamellar structure. The symmetry within the crystal and the angles between the imidazolium moieties and the alkyl chains give a unique S-like shape to the molecule. This class of diimidazolium salts cannot be described as a rod or cylinder-shaped molecule, but as one containing two 16 Å long cylinders linked to a smaller 10 Å cylinder with angles of 45° between them. The interpenetration of the alkyl sidechains is not complete, and a four-carbon gap can be observed. For example, the C4 of a side-chain is closer to the C8 of the next sidechain (Fig. 1).

The interaction between the imidazolium rings and the TfO anions are weak but can still be observed: an H-bond is observed between the H2 of the imidazolium ring and an oxygen atom of the triflate counterion. The calculated distance was 2.14 Å, which classifies this interaction as a moderate CH \cdots O hydrogen bond (Fig. 2).

The 3D organization of the *bis*(trifluoromethylsulfonyl)imide (NTf₂) salt **3a** is more complex: hydrophobic interactions govern the packing in one direction while the H-bonds and the electrostatic forces are the main interactions in another direction (Fig. 3). Furthermore, no π -stacking or T-stacking was observed either. The alkyl chains are separated from each other by 4.6 Å in the (*bc*) plane and only a two-carbon gap can be observed in the interpenetration of the sidechains. The two imidazolium cations of the dicationic core are still in a *trans* conformation relative to one another, and all the hydrogens (H2, H4 and H5) are involved in relatively weak H-bonds with the counterion (Fig. 4).

Four moderate to weak different hydrogen bonds can be observed in the crystal structure: the H2 and H4 of the imidazolium moieties are hydrogen bonded to an oxygen atom of the counterion (2.49 Å and 2.31 Å) while H5 is hydrogen bonded to a fluorine atom of the counterion (2.48 Å). There is also a

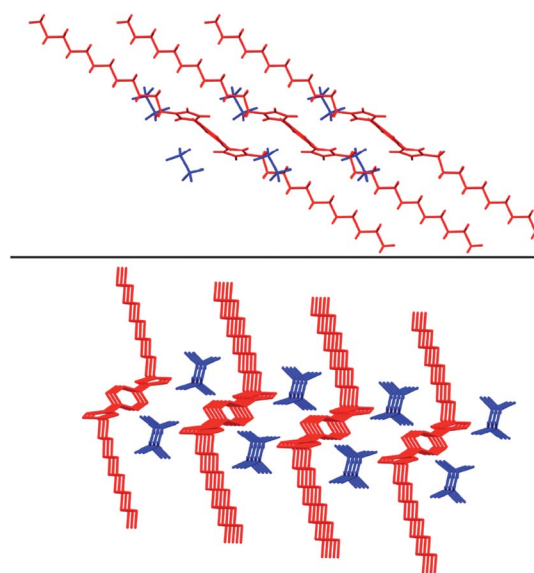


Fig. 1 Top: partial crystal packing of the compound **2a** projected on the (*bc*) plane showing the hydrophobic interactions in the crystal. Bottom: partial crystal packing of **2a** showing the lamellar structure.

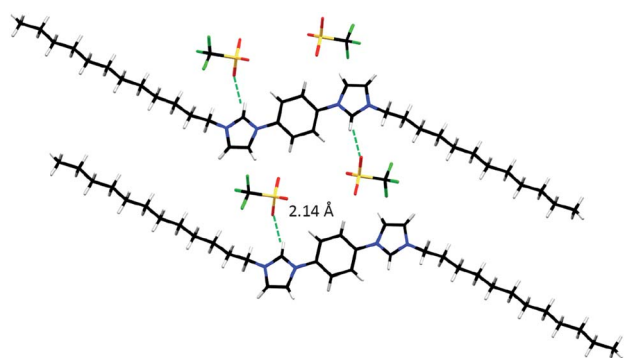


Fig. 2 Crystal structure of compound **2a** showing the supramolecular interactions between the imidazolium cations and the triflate anions.

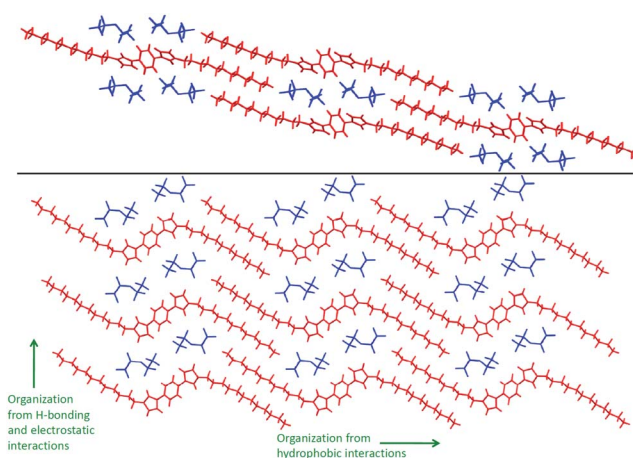


Fig. 3 Top: crystal packing of the compound **3a** projected on the (bc) plane showing the hydrophobic interactions. Bottom: crystal packing of **3a** showing the 2D organization.

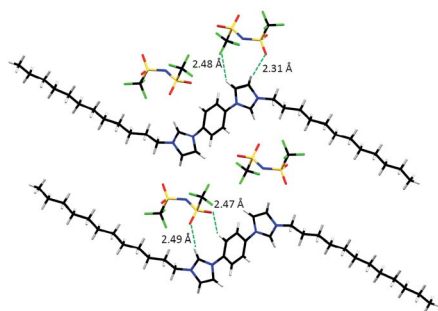


Fig. 4 Crystal structure of compound **3a** showing the supramolecular interactions between the imidazolium cations and the NTF₂ anions.

hydrogen bond between a proton of the central phenyl ring and an oxygen atom of the counterion (2.47 Å). This implies that every imidazolium moiety of the cationic core is surrounded by two anions and each anion is surrounded by 2 imidazolium rings. Furthermore, the distance between 2 anions surrounding the same imidazolium moiety is measured to be 11.4 Å. The higher 2D organization of **3a** compared to **2a** is also reflected in the mesogenic properties of these compounds.

Liquid crystal properties

While compounds **1a** and **1b** decompose before their fusion points, no other transition to a mesophase was observed before their decomposition. Thermogravimetric analyses of compounds **2a** and **2b**, and **3a** and **3b** showed that they were stable in a wide temperature range (ESI†). More precisely, compounds **2a** and **2b** started to degrade around 250 °C with the main degradation peak observable around 320 °C by TGA. However, if heated at or slightly above 250 °C and then cooled down, the mesomorphic properties were lost. Compounds **3a** and **3b**, on the other hand, were completely stable up to 350 °C.

The TfO salts **2a** and **2b** exhibited two phase transitions below the isotropic phase, while the NTF₂ salts **3a** and **3b** exhibited only one transition, but at a lower temperature. For all the compounds, their mesomorphic properties and phase transition temperatures were investigated by differential scanning calorimetry (DSC), polarizing optical microscopy (POM), and powder X-ray diffractometry (PXRD). To avoid hydration of the imidazolium salts, all the compounds were dried under vacuum before PXRD and DSC analyses (ESI†). The phase transition temperatures and the corresponding enthalpy changes derived for compounds **2a** and **2b**, and **3a** and **3b** in both heating and cooling cycles are shown in Table 1.

Results are summarized in Chart 1 for a visual comparison of the phase transition temperatures. For **2a** and **2b**, phase transitions were investigated by PXRD and POM (Fig. 5). Compound **2a** exhibited a fan-shaped texture often seen in SmC phases. This texture was observed on cooling from the isotropic melt between 181 and 153 °C.

Compound **2b** predominantly exhibited a focal conic fan texture upon cooling from the isotropic melt, but other types of 2D organization (e.g. a different orientation of the director of the focal conic aggregates) were also present simultaneously in the sample (Fig. 6). One sharp reflection in the small angle region related to the smectic layering, as well as a broad band in the wide angle region, related to the disordered alkyl chains and possibly

Table 1 Phase transition temperatures and corresponding enthalpies ΔH determined from 2nd heating and 1st cooling DSC thermograms

Compound	$T/^\circ\text{C}$ (Cr1 \rightarrow Cr2) on heating ^a	$T/^\circ\text{C}$ (Cr2 \rightarrow LC) ($\Delta H/\text{J g}^{-1}$)	$T/^\circ\text{C}$ (LC \rightarrow I) ($\Delta H/\text{J g}^{-1}$)
2a	148 (26.9)	169 (42.9)	184 (3.4)
2b	141 ^b	149	dec. at 250
3a	—	55 ^c (54.0)	136 (7.8)
3b	—	75 (48.8)	172 (6.8)

Compound	$T/^\circ\text{C}$ (Cr1 \rightarrow Cr2) on cooling	$T/^\circ\text{C}$ (Cr2 \rightarrow LC) ($\Delta H/\text{J g}^{-1}$)	$T/^\circ\text{C}$ (LC \rightarrow I) ($\Delta H/\text{J g}^{-1}$)
2a	110 (−27.2)	151 (−43.6)	183 (−3.3)
2b	104 (−30.9)	130 (−56.3)	dec. at 250
3a	—	46 (−28)	133 (−7.2)
3b	—	56 (−46.2)	169 (−4.9)

^a Abbreviations: Cr1 and Cr2 = crystalline phases, LC = liquid crystal phase, and I = isotropic phase. ^b $\Delta H = 83.9 \text{ J g}^{-1}$ was determined on heating for Cr1 \rightarrow Cr2 \rightarrow LC. The ΔH could not be determined for Cr1 \rightarrow Cr2 as well as for Cr2 \rightarrow LC due to the proximity of the transition temperatures. ^c For compound **3a**, a minor phase transition was observed ($\Delta H = 2.5 \text{ J g}^{-1}$) at 105 °C, between two smectic phases.

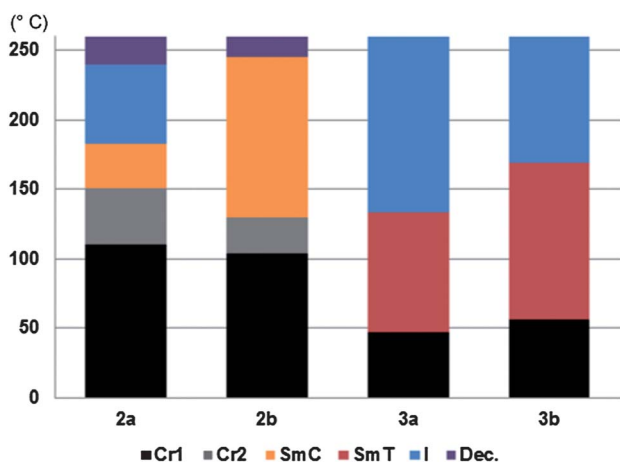


Chart 1 Phase transition temperatures of compounds **2a** and **2b** and upon cooling from the isotropic melt. Cr1 and Cr2: crystalline phases; SmC: smectic C mesophase; SmT: smectic T mesophase; I: isotropic phase; Dec: decomposition.

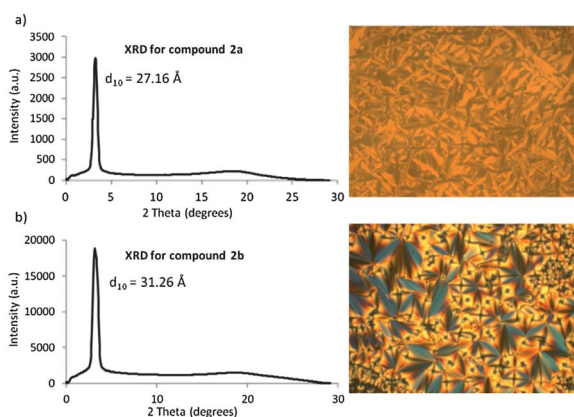


Fig. 5 (a) Left: XRD pattern of **2a** at 175 °C; right: $\times 200$ POM view of **2a** at 175 °C exhibiting a fan-shaped texture of a SmC phase. (b) Left: XRD pattern of **2b** at 170 °C; right: $\times 200$ POM view of **2b** at 170 °C exhibiting a focal conic fan texture of a SmC phase.

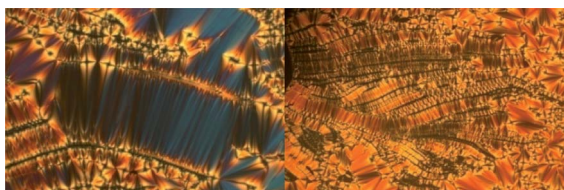


Fig. 6 Different textures observed by POM for compound **2b** in the same sample at 170 °C. Left: $\times 200$ view of a closely packed SmC phase. Right: $\times 100$ view showing the 2D organization at long range.

to liquid-like lateral correlations of the aromatic cores within the layers is seen. The d -spacing values obtained were $d = 26.8 \text{ \AA}$ for **2a** and $d = 31.3 \text{ \AA}$ for **2b**. In both cases, the d -spacing is shorter than the length of a single molecule ($d/L = 0.72$ for **2a** and $d/L = 0.67$ for **2b**), resulting in tilting which confirms the characterization of this mesophase as a SmC and an interdigitation of the alkyl chains within the mesophase. With these d -spacing values and the crystal structure of compound **2a** described above, we

can estimate that these TfO salts are organized in a monolayered SmC phase as shown in Fig. 7, with partial intercalation of the alkyl chains. The *trans* conformation of the diimidazolium salt also gives the liquid crystalline structure an inherent tilt angle. No secondary reflection is observed by PXRD, which implies that the counterions do not contribute to an organization in a second dimension, which is consistent with what was observed in the crystal structure of compound **2a**.

Compounds **3a** and **3b** present different mesomorphic properties compared to **2a** and **2b**. The structure of the mesophases was investigated by XRD and POM (Fig. 8). The mesophase had a wider temperature range, with smectic transitions starting as low as 46 °C for **3a**. These two NTf₂ salts can thus be described as ionic liquid crystals. A first sharp reflection with high intensity is observed followed by three more equidistant reflections of low intensity in the small angle region for **3a**. For compound **3b**, the first high intensity sharp reflection is followed by two equidistant reflections of low intensity. As previously seen for compounds **2a** and **2b**, the supramolecular forces involved in the formation of the smectic layers are predominantly hydrophobic interactions, but in this case there is at least another important interaction. This interaction can be either aromatic interactions or interactions between the acidic H2 proton of the imidazolium group and the anions. Since no aromatic interaction was observed in the crystal structure of **3a**, but significant H-bonds and electrostatic interactions were occurring between the imidazolium moieties

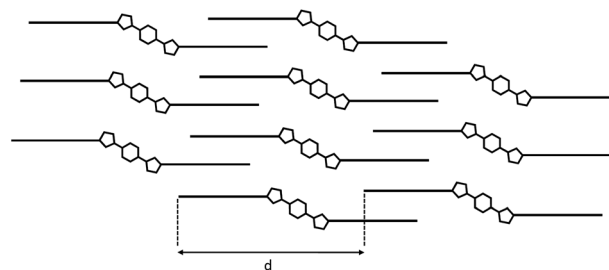


Fig. 7 Schematic representation of the organization of **2a** in the SmC mesophase.

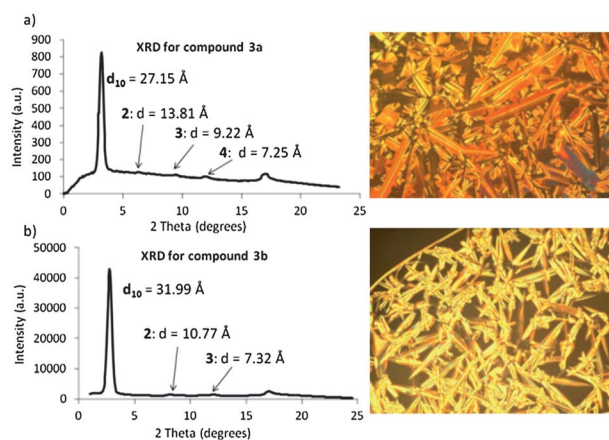


Fig. 8 (a) Left: XRD pattern of **3a** at 120 °C; right: $\times 100$ POM view of **3a** at 175 °C exhibiting a lancet-like texture of a SmT phase. (b) Left: XRD pattern of **3b** at 120 °C; right: $\times 100$ POM view of **3b** at 120 °C exhibiting a lancet-like texture of a SmT phase.

and the counterions, it is probable that interactions of the same nature occur in the mesophase. The anions can serve as bridges between the diimidazolium units and allow more cohesion in the structure, as shown in Fig. 9.

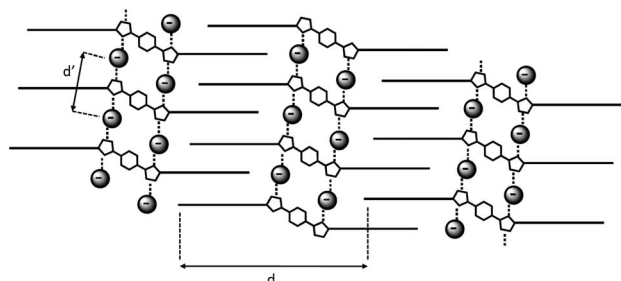


Fig. 9 Schematic representation of the organization of **3a** in the SmT mesophase.

For both compounds **3a** and **3b**, a slow growing lancet-like texture was observed upon cooling from the isotropic melt. This texture closely resembles that of growing crystals but both compounds can be described as viscous liquids after the first phase transition around 50 °C, which is a very common property of imidazolium ionic liquids in this temperature range. The same lancet-like texture has been reported also for Smectic T (SmT) mesophases.¹⁸ The peaks at around $2\theta = 17^\circ$ are slightly sharper than those of more commonly seen smectic A and C phases, which indicates that the alkyl sidechains are less amorphous and give to this SmT mesophase a soft crystalline nature. Furthermore, for compound **3a**, a transition between two different SmT phases was observed by DSC at 105 °C, with a ΔH of about 2.5 J g⁻¹. No change in the PXRD was observed, as the *d*-spacings remain the same, as well as the shape of the diffraction pattern. Only a slight difference is observed by POM between these two phases when cooling from the isotropic melt. As a result, we believe that we can correlate this to a minor reorganization of the SmT mesophase at 105 °C, but no further evidence of this reorganization was obtained. This phase transition was not observed for compound **3b** which has longer side-chains.

Ionic conductivity

As the liquid crystalline network formed by these salts can be seen as an anisotropically functional organization,¹⁹ the relationship between the mesomorphic behaviour and ionic conductivity was studied for compounds **2a**, **2b**, **3a** and **3b** (Table 2). For the same alkyl chain, a small conductivity decrease is noted with the increase of the anion size, as the TfO salts

Table 2 Ionic conductivities in the smectic and isotropic phases

Compounds	Conductivity in Sm phase (°C) ($\times 10^{-3}$ S cm ⁻¹)	Conductivity in I phase (°C) ($\times 10^{-3}$ S cm ⁻¹)
2a	0.38 (175 °C)	<i>n.d.</i> ^a
2b	0.67 (175 °C)	<i>n.d.</i> ^a
3a	0.28 (130 °C)	6.2 (175 °C)
3b	0.43 (130 °C)	8.2 (175 °C)

^a The temperature limit of our system was 175 °C.

present a higher conductivity than the NTF₂ salts, although very little difference in conductivity is observed compared to typical imidazolium-based ionic liquids made with these anions.¹⁹ For a given anion, a 1.5 to 1.7-fold increase in conductivity is obtained between the C₁₂ and C₁₆ sidechains which could indicate a less compact structure of the alkyl chain phase, allowing a faster ion transport across the phase. The highest ionic conductivity achieved was obtained in the SmC phase for **2b**. This conductivity is probably due to the diffusion of the anions inside the alkyl layers. When the temperature of the NTF₂ salts was raised above the smectic–isotropic transition, a strong increase in conductivity was observed as the ions gain freedom of movement in all directions. As reported for other imidazolium-based ILC, the ionic conductivities depend on the nature of the anion, but they present higher ionic conductivities than other imidazolium-based ILCs previously reported.¹⁹ The ionic conductivity in the Sm phase is 10 times lower than that in the best imidazolium-based ionogels recently described.^{9c} However their anisotropy and temperature controllable conductivities may open the door to the development of their application for photovoltaic fuel cells when doped with a lithium salt, or as matrix in the electrosynthesis of diverse materials.

Conclusions

We have investigated the mesomorphic properties of a new family of diimidazolium salts by varying the counterions and the length of the alkyl chains. The counterion has a great impact on the mesomorphism and the temperature of the phase transitions. Only SmC phases could be identified with the TfO counterion with a much larger range of liquid crystal phase for the longer C₁₆ alkyl sidechains. When symmetrical NTF₂ counterions were used, the first phase transition into a liquid crystalline phase occurs at around 50 °C, 120 °C lower than that of the TfO compounds. The ionic liquid crystalline phases obtained have been classified into SmT phases. The thermotropic mesomorphism of these ionic liquid crystals opens the possibility of using them as ordered solvents or organized reaction media. In these anisotropic solvents other chemo- and regioselectivities besides those in conventional solvents can be obtained for several types of reactions. The use of this type of ILCs for charge transport may find application in the fabrication of new electrochemical materials with temperature-controlled conductivities.

Experimental section

All commercially available chemicals were used without further purification. Nuclear Magnetic Resonance (NMR) experiments were done either on a Brüker Avance AV400 operating at 400 MHz for ¹H NMR experiments and at 100 MHz for ¹³C NMR experiments or on a Brüker Avance AV300 operating at 75 MHz for ¹³C NMR experiments. Electrospray Ionisation (ESI) mass spectra were recorded with a TSQ Quantum Ultra (Thermo Scientific) Mass Spectrometer with accurate mass options instrument (Université de Montréal Mass Spectrometry Facility). Differential scanning calorimetry (DSC) analyses were carried out on a Q2000 TA instruments. X-ray diffraction (XRD) studies were carried out on a Brüker D8 Discover,

equipped with a Hi-Star detector. XRD data were collected using GADDS 4.1.1.4 software and EVA 8.0.0.2 was used for data analysis. A custom made XYZ stage with a temperature control chamber and a Cu source (K_{α} energy of 8.04 keV and $\lambda = 1.541838 \text{ \AA}$) were used. Polarizing optical microscopy (POM) was carried out with a Zeiss Axioskop 40Pol microscope coupled with a Linkam Scientific Instrument THMS600 hot stage and a TMS94 temperature controller.

1-[4-(1*H*-imidazol-1-yl)phenyl]-1*H*-imidazole was synthesized following a previously reported procedure.²⁰ The ^1H and ^{13}C NMR spectra of this compound were found to be in accordance with the literature.

General procedure for the synthesis of dialkyl(1,4-phenylene) diimidazolium salts

To a solution of 1-[4-(1*H*-imidazol-1-yl)phenyl]-1*H*-imidazole (1 mmol, 210 mg, 1 eq.) in acetonitrile (10 mL) was added the appropriate alkyl bromide (10 mmol, 10 eq.). The solution was refluxed and stirred for 24 h and then filtered. The diimidazolium bromide salts were dried under high vacuum for 24 h then solubilised in 10 mL of methanol. Either lithium *bis*(trifluoromethylsulfonyl)imidate or ammonium triflate (2.1 mmol, 2.1 eq.) was added and the solution was refluxed for 2 h. After evaporation of the solvent, water was added and the subsequent salts were filtered and dried under high vacuum.

1,1'-Didodecyl-3,3'-(1,4-phenylene)diimidazolium *bis*(triflate) (**2a**): ^1H NMR (CD_3OD , 400 MHz): δ (ppm) 8.21 (s, 2H), 8.07 (s, 4H), 7.95 (s, 2H), 4.37 (t, $J = 7.4 \text{ Hz}$, 4H), 2.08 (sext, $J = 6.1 \text{ Hz}$, 4H), 1.27–1.53 (m, 36H), 0.91 (t, $J = 6.06 \text{ Hz}$, 6H). ^{13}C NMR (CD_3OD , 100 MHz): δ (ppm) 135.6, 123.5, 123.0, 121.1, 49.8, 31.3, 29.2, 29.0, 28.9, 28.7, 28.6, 28.3, 25.6, 21.9, 12.6. HR-MS m/z found: 274.2412 ($[\text{M} - 2\text{TfO}]^{2+}$), calc.: 274.2403. Elem. analysis: found: 6.52% N, 54.20% C, 7.40% H, 7.32% S; calc.: 6.61% N, 53.83% C, 7.08% H, 7.56% S, yield 88%.

1,1'-Dihexadecyl-3,3'-(1,4-phenylene)diimidazolium *bis*(triflate) (**2b**): ^1H NMR (CD_3OD , 400 MHz): δ (ppm) 8.21 (s, 2H), 8.07 (s, 4H), 7.95 (s, 2H), 4.37 (t, $J = 7.4 \text{ Hz}$, 4H), 2.03 (m, 4H), 1.25–1.51 (m, 52H) 0.92 (t, $J = 6.6 \text{ Hz}$, 6H). ^{13}C NMR (CD_3OD , 100 MHz): δ (ppm) 135.6, 123.5, 123.0, 121.1, 49.8, 31.3, 29.2, 29.0, 28.9, 28.7 (multiple peaks), 28.6, 28.3, 25.6, 21.9, 12.6. HR-MS m/z found: 330.3045 ($[\text{M} - 2\text{TfO}]^{2+}$), calc.: 330.3029. Elem. analysis: found: 5.85% N, 57.40% C, 7.99% H, 5.95% S; calc.: 5.84% N, 57.54% C, 7.92% H, 6.67% S, yield 71%.

1,1'-Didodecyl-3,3'-(1,4-phenylene)diimidazolium *bis*[*bis*(trifluoromethane-sulfonyl)imide] (**3a**): ^1H NMR (CD_3OD , 400 MHz): δ (ppm) 8.18 (d, $J = 1.4 \text{ Hz}$, 2H), 8.05 (s, 4H), 7.93 (d, $J = 1.4 \text{ Hz}$, 2H), 4.36 (t, $J = 7.4 \text{ Hz}$, 4H), 2.03 (m, 4H), 1.27–1.50 (m, 36H), 0.91 (t, $J = 6.79 \text{ Hz}$, 6H). ^{13}C NMR (CD_3OD , 100 MHz): δ (ppm) 135.6, 123.6, 123.1, 121.1, 49.8, 31.3, 29.2, 29.0, 28.8, 28.7, 28.6, 28.3, 25.5, 21.9, 12.6. HR-MS m/z found: 274.2411 ($[\text{M} - 2\text{NTf}_2]^{2+}$), calc.: 274.2403. Elem. analysis: found: 7.52% N, 43.49% C, 5.62% H, 11.67% S; calc.: 7.57% N, 43.27% C, 5.41% H, 11.53% S, yield 83%.

1,1'-Dihexadecyl-3,3'-(1,4-phenylene)diimidazolium *bis*[*bis*(trifluoromethane-sulfonyl)imide] (**3b**): ^1H NMR (CD_3OD , 400 MHz): δ (ppm) 8.19 (d, $J = 1.4 \text{ Hz}$, 2H), 8.06 (s, 4H), 7.94 (d, $J = 1.4 \text{ Hz}$, 2H), 4.36 (t, $J = 7.3 \text{ Hz}$, 4H), 2.03 (m, 4H), 1.25–1.51 (m, 52H) 0.92 (t, $J = 6.6 \text{ Hz}$, 6H). ^{13}C NMR (CD_3OD , 75 MHz): δ

(ppm) 133.8, 124.8, 124.3, 122.3, 118.5, 51.0, 32.5, 30.4, 30.2 (multiple peaks), 30.1, 30.0, 29.9, 29.8, 29.5, 26.7, 23.1, 13.8. HR-MS m/z found: 330.3043 ($[\text{M} - 2\text{NTf}_2]^{2+}$), calc.: 330.3029. Elem. analysis: found: 6.71% N, 46.38% C, 6.28% H, 10.06% S; calc.: 6.88% N, 47.15% C, 6.22% H, 10.47% S, yield 67%.

Ionic conductivity

Ionic conductivities were measured with a two-probe setup using a cell made in house. This cell consisted of two 0.25 mm Pt wires (Alfa Aesar 99.9%) protruding from a glass tube and separated from each other by *ca.* 2 mm. Electrochemical impedance spectra (PARSTAT 2273) were recorded for the samples heated at various temperatures (oil bath) from 10^{-3} to 10^5 Hz at open circuit potential. The cell resistance was determined from the intercept of the curve on the real impedance axis of the Nyquist plots at high frequencies. The cell was thereby calibrated with a KCl conductivity standard solution (Alfa Aesar, $15\,000 \mu\text{S cm}^{-1}$) to obtain the conductivity of the ILCs.

Acknowledgements

We thank the Natural Sciences and Engineering Research Council of Canada (NSERC), the Fonds Québécois pour la Recherche, la Nature et les Technologies (FQRNT), the Canada Foundation for Innovation (CFI) and Université de Montreal for financial support. We thank S. Essiembre for the help in the use of the powder X-ray diffractometer, P. Ménard-Tremblay for his help on POM and M. Simard for XRD diffraction. We would also like to thank Professor G. Bazuin for her help with identification of the liquid crystalline phases.

Notes and references

- (a) P. Wasserscheid and T. Welton, *Ionic Liquids in Synthesis*, Wiley-VCH, Weinheim, 2003; (b) J. Dupont, R. F. de Soula and P. A. Suarez, *Chem. Rev.*, 2002, **102**, 3667.
- H. Ohno, *Electrochemical Aspect of Ionic Liquids*, Wiley-Interscience, 2005.
- V. Gauchot, W. Kroutil and A. R. Schmitzer, *Chem.–Eur. J.*, 2010, **16**, 6748.
- L. Leclercq, M. Lacour, S. H. Sanon and A. R. Schmitzer, *Chem.–Eur. J.*, 2009, **15**, 6327.
- (a) H. Ohno, M. Yoshizawa and W. Ogihara, *Electrochim. Acta*, 2004, **50**, 255; (b) H. Ohno, *Electrochim. Acta*, 2001, **46**, 1407; (c) A. Noda and M. Watanabe, *Electrochim. Acta*, 2000, **45**, 1265; (d) M. Watanabe and T. Mizumura, *Solid State Ionics*, 1996, **86–88**, 353.
- (a) A. Lewandowski and A. Swiderska, *Solid State Ionics*, 2004, **169**, 21; (b) J. Fuller, A. C. Breda and R. T. Carlin, *J. Electroanal. Chem.*, 1998, **459**, 29.
- J. Sun, D. R. MacFarlane and M. Forsyth, *Solid State Ionics*, 2002, **147**, 333.
- J. Fuller, A. C. Breda and R. T. Carlin, *J. Electrochem. Soc.*, 1997, **144**, L67.
- (a) J. Le Bideau, L. Viau and A. Vioux, *Chem. Soc. Rev.*, 2012, **2**, 907; (b) J. Casamada Ribot, C. Guerrero-Sanchez, T. L. Greaves, D. F. Kennedy, R. Hoogenboom and U. S. Schubert, *Soft Matter*, 2012, **8**, 1025; (c) J. Casamada Ribot, C. Guerrero-Sanchez, R. Hoogenboom and U. S. Schubert, *J. Mater. Chem.*, 2010, **20**, 8279.
- (a) K. M. Lee, Y. T. Lee and J. B. Lin, *J. Mater. Chem.*, 2003, **13**, 1079; (b) J. De Roche, C. M. Gordon, C. T. Imrie, M. D. Ingram, A. R. Ingram, A. R. Kenedy, F. LoCelso and A. Triolo, *Chem. Mater.*, 2003, **15**, 2003; (c) S. Kumar and S. Kumar Pal, *Tetrahedron Lett.*, 2005, **46**, 2607; (d) J. Motoyagani, T. Fukushima and T. Aida, *Chem. Commun.*, 2005, 101; (e) J. M. Suisse, S. Bellemin-Laponnaz, L. Douce, A. Maise-François and

- R. Welter, *Tetrahedron Lett.*, 2005, **46**, 4303; (f) K. Binnemans, *Chem. Rev.*, 2005, **105**, 4148.
- 11 W. Dobbs, L. Douce, L. Allouche, A. Louati, F. Malbosc and R. Welter, *New J. Chem.*, 2006, **30**, 528.
- 12 (a) C. K. Lee, H. W. Huang and I. J. B. Lin, *Chem. Commun.*, 2000, 1911; (b) M. Tosoni, S. Laschat and A. Baro, *Helv. Chim. Acta*, 2004, **87**, 2742; (c) Y. R. Zhao, X. Chen and X. D. Wang, *J. Phys. Chem. B*, 2009, **113**, 2024; (d) M. Yoshio, T. Mukai, K. Kanie, M. Yoshizawa, H. Ohno and T. Kato, *Chem. Lett.*, 2002, 320.
- 13 X. Cheng, X. Bai, S. Jing, H. Ebert, M. Prehm and C. Tschierske, *Chem.–Eur. J.*, 2010, **16**, 4588.
- 14 (a) S. Yazaki, Y. Kamikawa, M. Yoshio, A. Hamasaki, T. Mukai, H. Ohno and T. Kato, *Chem. Lett.*, 2008, **38**, 538; (b) K. Hoshino, M. Yoshio, T. Mukai, K. Kishimoto, H. Ohno and T. Kato, *J. Polym. Sci., Part A: Polym. Chem.*, 2003, **41**, 3486; (c) M. Yoshio, T. Mukai, H. Ohno and T. Kato, *J. Am. Chem. Soc.*, 2004, **126**, 994.
- 15 (a) Y. Sanami, M. Funahashi and T. Kato, *J. Am. Chem. Soc.*, 2008, **130**, 13206; (b) L. Chui and L. Zhu, *Liq. Cryst.*, 2005, **32**, 143.
- 16 N. Noujeim, B. Jouvelet and A. R. Schmitzer, *J. Phys. Chem. B*, 2009, **113**, 16159.
- 17 (a) L. Leclercq, N. Noujeim and A. R. Schmitzer, *Cryst. Growth Des.*, 2009, **9**, 4784; (b) L. Leclercq, M. Simard and A. R. Schmitzer, *J. Mol. Struct.*, 2009, **918**, 101.
- 18 (a) E. Alami, H. Levy, R. Zana, P. Weber and A. Scoulios, *Liq. Cryst.*, 1993, 201–212; (b) K. Goossens, K. Lava, P. Nockemann, K. Van Hecke, L. Van Meervelt, K. Driesen, C. Garller-Walrand, K. Binnemans and T. Cardinaels, *Chem.–Eur. J.*, 2009, **15**, 656.
- 19 (a) J. Pitawala, A. Matic, A. Martinelli, P. Jacobsson, V. Koch and F. Croce, *J. Phys. Chem. B*, 2009, **113**, 10607; (b) H. Tokuda, K. Ishii, A. B. H. Susan, S. Tsuzuki, K. Hayamizu and M. Watanabe, *J. Phys. Chem. B*, 2006, **110**, 2833; (c) M. Yoshio, T. Ichikawa, H. Shimura, T. Kagata, A. Hamasaki, T. Mukai and T. Kato, *Bull. Chem. Soc. Jpn.*, 2007, **9**, 1836.
- 20 H.-J. Cristau, P. P. Cellier, J.-F. Spindle and M. Taillefer, *Chem. Eur. J.*, 2004, **10**, 5607–5622.